Symmetric Diblock Copolymer Thin Films on Rough Substrates: Microdomain Periodicity in Pure and Blended Films

Easan Sivaniah,[†] Shinya Matsubara, Yue Zhao,[‡] and Takeji Hashimoto*,[‡]

Department of Polymer Chemistry, Graduate School of Engineering, Kyoto University, Katsura, Kyoto 615-8510, Japan

Kenji Fukunaga

Polymer Lab UBE Ind Ltd., 8-1 Goi Minamikaigan, Chiba 2900045, Japan

Edward J. Kramer and Tom E. Mates

Materials Department, University of California at Santa Barbara, Santa Barbara, California 93106

Received November 7, 2007; Revised Manuscript Received January 14, 2008

ABSTRACT: The lamellar dimension, D, for pure and blended block copolymer (BCPs) thin films of symmetric poly(styrene)-*block*-poly(methyl methacrylate) was measured using atomic force microscopy analysis of surface patterns of perpendicularly oriented lamellar structures. It was approximately verified, using SAXS and AFM analysis, that perpendicular structures in lamellar thin films bounded by a neutral and a roughened interface did not significantly alter the bulk block copolymer phase separation thermodynamics. In the case of blends, it was also verified that there was a uniform distribution of blend components throughout the thin film. These checks allowed a detailed comparison of D as a function of the number of statistical segments (N) and blend composition using existing bulk phase predictions and experiments. In pure BCPs we observed the two characteristic regimes; strong ($D \sim N^{0.66}$) and intermediate segregation regimes ($D \sim N^{0.85}$). In addition, we observed a more complicated, weakly segregated regime where D does not scale as $N^{0.5}$ as expected for a random coil. In blended BCPs there was good agreement with existing theory when BCP components from the strongly segregated regime were used. In cases where intermediate or weakly segregating BCP components were used, an alternative semiempirical analytical function was developed. In cases where the ratio of N for the BCP blend components exceeds ∼5, macrophase separation was observed in the thin film with the smaller BCP component remaining at the air surface.

1. Introduction

Block copolymers (BCPs) are celebrated for the intrinsic ability to self-assemble to provide nanostructural architectures in relatively few, simple processing steps. Since the BCPs contain polymeric components that are often mutually immiscible, the BCP undergoes microphase separation (forming ordered phases) at the molecular level, creating microdomains of virtually pure components. One can control the length scale at which different chemical components are separated as well as the complexity of the microphase-separated architecture. The resulting material properties can be superior to those of homopolymeric blends with a macrophase-separated morphology.

Control of the size of the microphase-separated domains is often essential[1] and is provided by two principal means: by chemically synthesizing a pure BCP of the correct molecular weight and by the blending of two chemically similar BCPs of large and small molecular weight to achieve an intermediately sized microdomain.[2]

The characteristic period of pure symmetric BCPs are often quoted as a function of N, the total number of monomeric statistical units, and χ, a temperature-dependent interaction parameter. In the strong segregation regime (SSR), at the limit of large χN, mean-field theory[3,4] suggests that D varies as $\chi^{1/6}N^{2/3}$. The 2/3 power law in the SSR has been demonstrated experimentally with polystyrene-*block*-isoprene by Hashimoto and co-workers[5] and verified for other BCP systems by numerous groups.[6–10] At the weak segregation limit (WSR), as χN is reduced to values where the BCP is expected to become homogeneous, D should scale as the dimension of a random coil, $N^{1/2}$.

There is some disagreement over what happens at the crossover between the weak and strongly segregating regimes. Within this so-called intermediate segregation regime (ISR), it is difficult to find an analytical solution to the BCP equilibrium conformation that accounts for the effects of near-critical fluctuations. Variational mean-field solutions have revealed a power law dependence of N^{ω}, where ω varies from 0.72 to 1.017.[11–14] Experimentally in the ISR, the observed ω is more consistent (0.8−0.83) through a range of different BCP systems.[6,8,15,16] The range of χN over which the three different regimes are dominant appears to be model dependent in theory and system dependent in experiments. For example, the ISR to SSR transition is predicted or observed to occur at a χN value that range from ∼30 to ∼100.[12,17,18] There is greater agreement for the WSR to ISR transition to occur at $\chi N \sim 15$.[8,12,16,18] Of the mentioned experimental works, Papadakis et al.[8] are the first to represent all three experimental regimes in a single plot and the only ones to experimentally report a transition from ISR to SSR (at $\chi N \sim 29$). In this paper, we will compare these findings to our data for the lamellar periodicities of pure BCPs of polystyrene-*block*-poly(methyl methacrylate) (PS-*b*-PMMA).

Blending a large and small BCP together in the appropriate ratio to produce a desired nanostructural dimension is more practically appealing than resynthesizing a pure BCP of the correct size. Therefore, it is convenient to be able to predict how blends of similar BCPs behave. Such theories were initiated

* Corresponding author.
[†] Present address: Department of Physics and Astronomy, Leeds University, Leeds, England LS2 9JT.
[‡] Present address: Advanced Science Research Center, Japan Atomic Energy Agency, Tokai-mura, Naka-gun, Ibaraki Pref. 319-1195, Japan.

10.1021/ma702465t CCC: $40.75
Published on Web 03/13/2008

Table 1. Pure BCPs Used in This Study and the Corresponding Lamellar Structure Size

polymer ID	N	D^a (nm)	D^b (nm)
15K−13K PS-*b*-PMMA	274	20 ± 1	21.2 ± 1
18K−18K PS-*b*-PMMA	353	28.6 ± 1	30.3 ± 1
25K−26K PS-*b*-PMMA	500	31.3 ± 1	33.8 ± 1
38K−37K PS-*b*-PMMA	735	36.7 ± 1	
37K−46K dPS-*b*-PMMA	790	40.2 ± 1	
50K−54K PS-*b*-PMMA	1021	43.5 ± 1	
70K−71K PS-*b*-PMMA	1383	63 ± 2	
85K−91K PS-*b*-PMMA	1727	74.7 ± 2	75.6 ± 1
106K−99K PS-*b*-PMMA	2009	98.2 ± 3	
170K−168K PS-*b*-PMMA	3315	137 ± 3	

[a] From AFM power spectral analysis. [b] From SAXS/USAXS analysis.

by Hashimoto, Zhulina, Bershtein, Spontak, and Matsen.[19–22] An analytical prediction for the lamellar dimension of a mixture of two symmetric SSR-type BCPs has been verified by many groups.[23–26] This prediction is a function of the number of statistical segments in the short (S) and long (L) BCPs, N_S and N_L, respectively, and the mole fraction of long chains in the mixture, x_L. It was shown that D_{mix}, the lamellar period of the mixture, can be expressed in terms of the Kuhn length (a), D_L, x_L, and α ($=N_S/N_L$)

$$D_{mix} = 2aN_L^{1/2}\left(\frac{8\chi N_L}{3\pi^4}\right)^{1/6} \times [\alpha + x_L(1-\alpha)][\alpha + x_L^{\upsilon+1}(1-\alpha)]^{-1/(\upsilon+1)}$$

or

$$D_{mix} = D_L[\alpha + x_L(1-\alpha)][\alpha + x_L^{\upsilon+1}(1-\alpha)]^{-1/(\upsilon+1)} \quad (1)$$

In this SSR analysis, the parameter υ has a value of 2 and the lamellar period, $D_{L(S)}$, scales as $N_{L(S)}^{\upsilon/(\upsilon+1)}$, indicating that both BCP components obey the 2/3 power rule. An examination of eq 1 shows that it will fail at $x_L = 0$ if one of the blend components is not a SSR BCP. In this paper we will explore the overall applicability of eq 1 in such cases.

The majority of our data is harvested from the AFM analysis of the surface structures of perpendicularly oriented BCP lamellae in a thin film. This method derives from an earlier observation by our group that such perpendicularly oriented lamellar BCPs were possible through the use of a suitably roughened substrate.[27] Although some papers have reported systematically determined lamellar periods in pure and blended BCP thin films,[10,28–31] the comparison of lamellar periodicity in thin films to those in the bulk is not a simple one. The principal complication is the altered thermodynamics in the thin film either through confinement by the film[32] or through the effects of the surface or substrate interfacial tension.[33,34] Thin film surfaces can induce surface segregation of one component in a blended BCP, again complicating the comparison to uniformly mixed bulk BCP states. Such considerations will be explored when comparing our results to contemporary reports that use bulk phase BCPs.

2. Substrate and Sample Preparation and Analysis

In our previous study[35] the use of substrates with roughness above a critical value always resulted in the perpendicular orientation of PS-*b*-PMMA lamellae throughout the polymer thin film. The substrate material was either float glass with a thermally deposited indium tin oxide (ITO) coating or a cured polyimide (PIM) surface that had been templated from the rough ITO surface. With reference to our earlier work, only supercritically rough substrates of ITO (SC_ITO) or PIM (SC_PIM) are used in this current study.

We obtained anionically synthesized symmetric PS-*b*-PMMA diblocks (Polymer Source Inc., Canada) of different molecular weights with low polydispersities ($M_w/M_n < 1.06$). The BCPs used are specified by including the molecular weights of each block in kilodaltons, e.g. 18K−18K PS-*b*-PMMA. A range of molecular weights were studied and are listed in Table 1. An additional BCP dPS-*b*-PMMA(37K–43K) containing a deuterated PS block was also used for ion beam depth profiling experiments.

Pure and blended solutions of BCPs were made using toluene as a solvent. In the case of blends, binary sets of BCP were weighed together in appropriate ratios before being cosolvated by toluene. BCP thin films of various thicknesses (ranging from 300 to 500 nm) were spun-cast from toluene solutions onto the substrates discussed above and dried overnight (at 60 °C) before annealing in a nitrogen-purged oven. Provided the thickness exceeded D or D_L (in the case of blends), the film's thickness was not considered to significantly alter the behavior of perpendicular lamellae. With one exception these thin film samples were annealed at 220 °C for 12 h and quickly quenched to room temperature by immersion in liquid nitrogen (LN_2). In the exception, the 14.9K−13.1K PS-*b*-

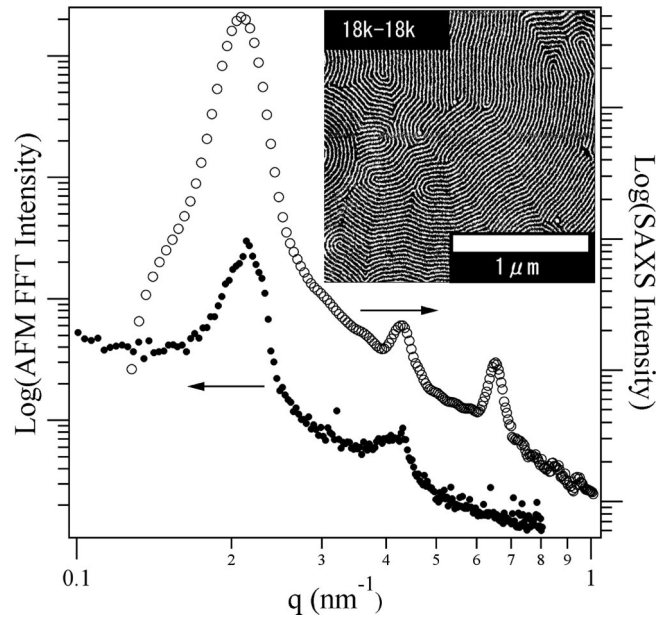

Figure 1. Comparison of AFM-derived power spectral density data (closed circles) and SAXS derived scattering data (open circles) for PS-*b*-PMMA(18K−18K). Inset: a typical AFM image used to generate the PSD.

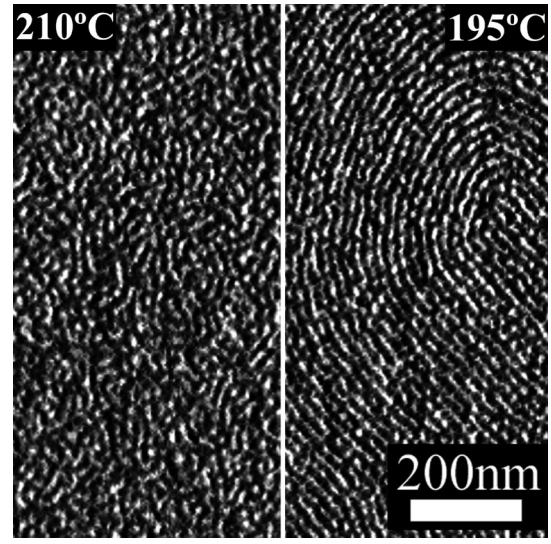

Figure 2. Comparison of AFM images of 14.9K−13.1K PS-*b*-PMMA at temperatures just above the T_{ODT} (left) and just below the T_{ODT} (right).

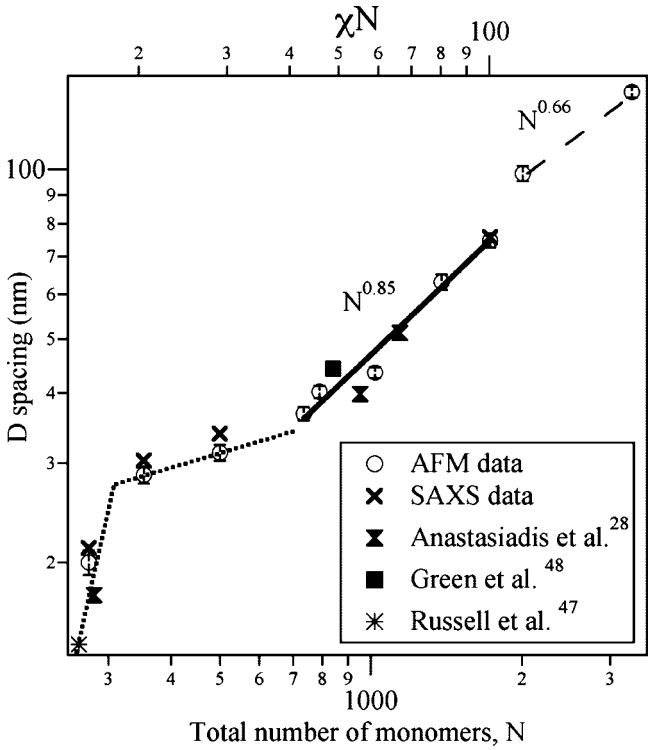

Figure 3. A cumulative plot of AFM and SAXS determined D vs N (bottom axis) and D vs χN (top axis). The dashed and solid lines are power law fits of D vs N with the best fit exponents listed in the graph. Also given are data points taken from comparative research in publication. A dotted line shows a kink behavior at low χN.

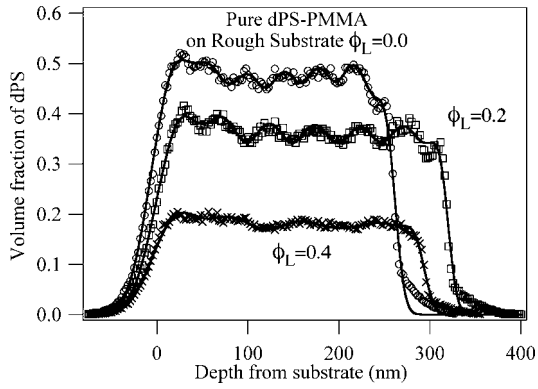

Figure 4. dSIMS profiles of pure dPS-*b*-PMMA and its blends with PS-*b*-PMMA(106K−99K) in different proportions.

PMMA thin film sample was annealed at 195 °C for the same amount of time. The lower temperature was necessary as this BCP becomes disordered at around 205 °C.

The sample structure was observed with tapping mode atomic force microscopy (AFM), transmission electron microcopy (TEM), dynamic secondary ion mass spectrometry (dSIMS), and small-angle X-ray scattering (SAXS).

In a typical AFM analysis, the BCP surface image was determined (using a Nanoscope III Multimode, from Digital Instruments, Santa Barbara, CA). Using accompanying AFM software, a 2-dimensionally averaged fast-Fourier analysis generated a power spectral distribution (PSD) (see Figure 1). The lamellar period, D, was extracted from a Gaussian fit of the principal peak position in the PSD distribution. Thermal drift and noise could lead to differences in the rates that the AFM tip scans along the vertical and horizontal axes (the so-called slow- and fast-scan axes).[36] To our approximation, this would lead to a broadening of the peak without altering its position. The standard deviation associated with

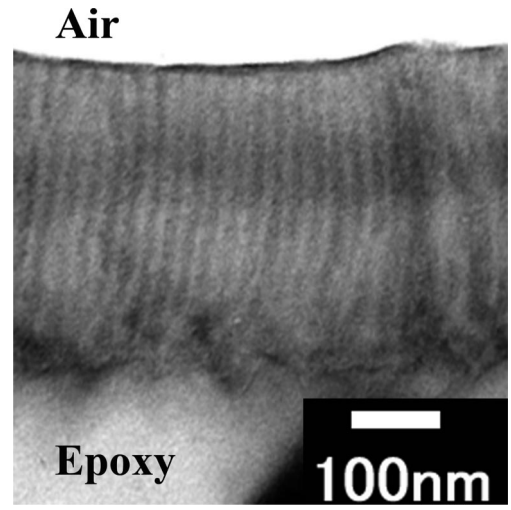

Figure 5. Thin film TEM cross section of a (ϕ_L = 0.2) blend of 37K−46K dPS-*b*-PMMA and 106K−99K PS-*b*-PMMA.

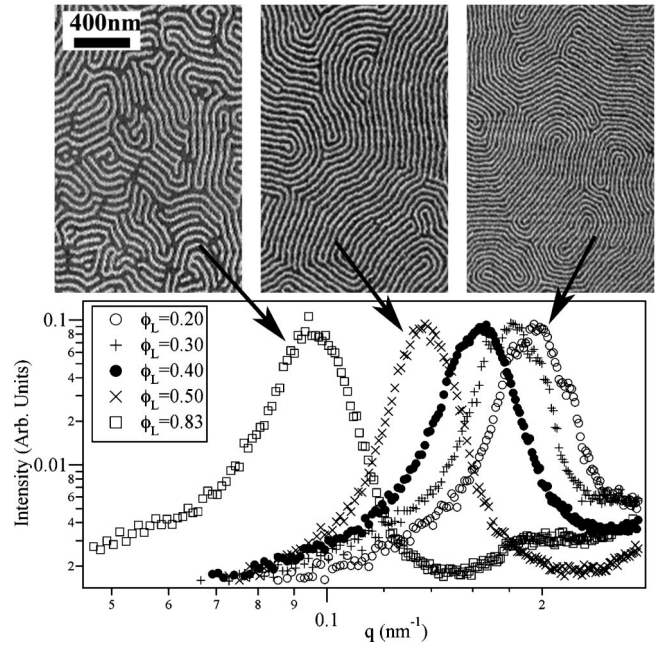

Figure 6. The upper panel shows slices of AFM images from the blend of 18K−18K PS-*b*-PMMA and 85K−91K PS-*b*-PMMA where ϕ_L = 0.83, 0.50, and 0.20 (for images from left to right). The lower panel shows the PSD analysis of these images along with PSD for blends where ϕ_L = 0.30 and 0.40.

the measurement of D was determined (to the nearest nanometer) using five measurements of D on each molecular weight BCP. These values are shown in Table 1, indicating a larger variation for the higher molecular weight samples. For the treatment of error in the blend samples, this variation in error was assumed linearly related to molar composition, i.e., $\Delta_{D,blend} = \Delta_{D,Long}x_L + \Delta_{D,Short}(1 - x_L)$, where Δ is the error associated with measurement of D. Thus, the error bars shown in Figures 7−10 are based on the pure BCP error values and are an approximate guide.

For TEM observation, the PS-*b*-PMMA film was released from the ITO substrate (by etching out via immersion in HCl) and picked up on a pre-cross-linked epoxy surface. The epoxy assembly was then cut in ultrathin (∼50 nm) cross sections using a Reichert-Nissei Ultracut-S cryo-ultramicrotome using methodologies described previously.[37] A JEOL (JEM2000FXZ) (JEOL, Tokyo, Japan) transmission electron microscope operated at 120 kV was used for observation of the cross sections. For better TEM contrast, these sections were stained by exposure to RuO_4 vapor

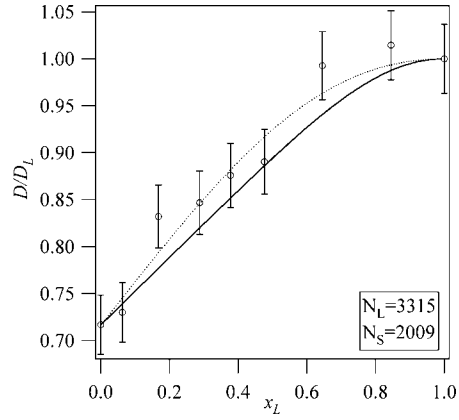

Figure 7. Lamellar period, D_{mix}, for a blend of two SSR BCPs. The dotted line is the SSR-based eq 1 with no adjustable experimental parameters. The solid line is a fit using a modified definition of α' and with the exponent $\upsilon/(\upsilon + 1)$ as 4/5.

so that the styrene block of the PS-*b*-PMMA appears darker in our figures.

dSIMS analysis was carried out on blended thin films containing dPS-*b*-PMMA annealed on PIM based rough substrates; the conductive ITO substrates tended to lead to unstable charging during sample analysis. A full description of the dSIMS procedure and instrument (Physical Electronics 6650 dynamic SIMS) is given elsewhere.[35,38]

Small-angle and ultrasmall-angle X-ray scattering on bulk PS-*b*-PMMA was performed using in-house equipment at our laboratory in Kyoto University. Thick samples (~1 mm) of PS-*b*-PMMA (four molecular weights were used from the available sample set) were solvent cast from toluene over a period of a week before vacuum-drying overnight at 60 °C. A full description of the typical SAXS instrumentation and analysis procedure used in the Hashimoto laboratory is provided elsewhere.[39] The presented SAXS profiles were corrected for air scattering, absorption, and thermal diffuse scattering.[40–42] Bulk SAXS or USAXS data of the four BCP samples were collected at 220 °C and used to determine the bulk lamellar period at this temperature.

3. Results and Discussion

3.1. Comparison of Bulk and Thin Film Behavior. This paper principally compares the lamellar period (measured at the air surface of thin films of perpendicularly oriented BCP) to predictions made for bulk phase BCP systems. Is this a valid comparison? Certainly Menelle et al. and Foster et al. have shown that the air surface of a parallel oriented BCP thin film becomes ordered at temperatures where the interior of the same film remains disordered and bulklike.[33,34] Equally, it is known that lamellar period of BCPs in a parallel orientation undergoes some elongation or compression in order to prevent the onset of island−hole formation.[31,32] However, these studies have all involved a parallel orientation of the BCP where there is a significant difference between the substrate/surface wetting power of the BCP components. In our experiments the thin films are bounded by a nearly neutral air surface and a supercritically rough substrate surface. The analogous experiments to those of Menelle et al. using neutral boundary conditions have yet to be reported. However, we believe that our boundary conditions act to create a neutral thin film interface so that the BCP thin film appears to be residing in a bulk phase. Moreover, there should be no entropic constraint by the thin film's thickness on the BCP chains that lie in the plane of the film. Critically, the following two suppositions must be tested: that the perpendicularly oriented BCPs bounded with neutral walls behave with bulk phase thermodynamics and that the thin film BCP *D* spacing was unaltered from the bulk state.

Using SAXS and USAXS, we determined the bulk phase *D* spacing of a select four symmetric PS-*b*-PMMA BCPs. These

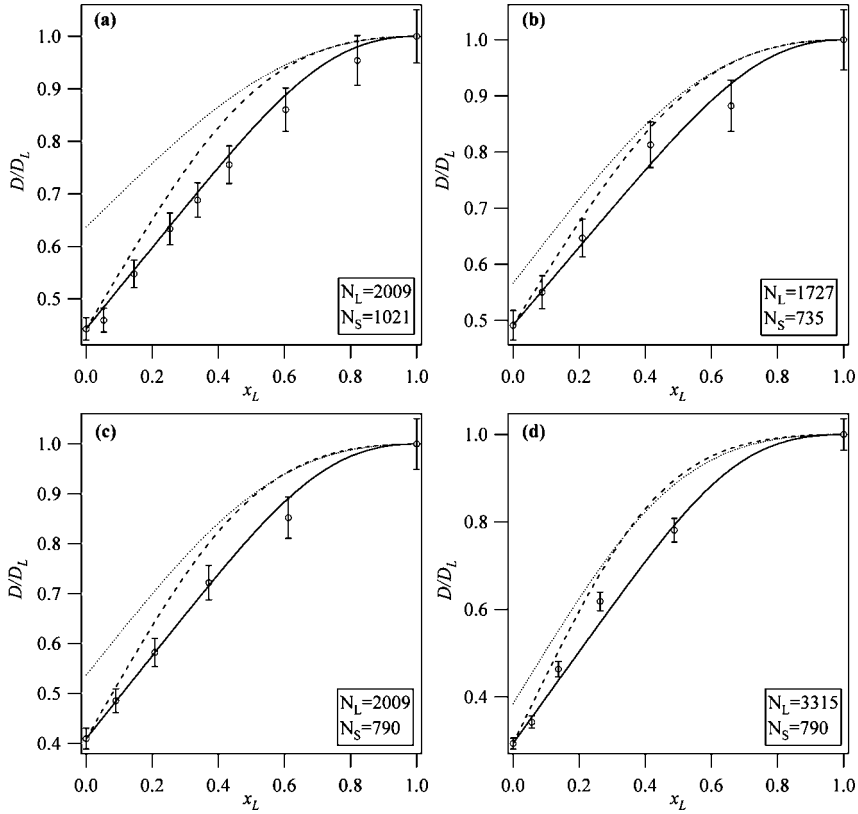

Figure 8. Lamellar period, D_{mix}, for blends where the smaller BCP is from the ISR. The dotted line is the SSR based eq 1 with no adjustable experimental parameters. The dashed line is a fit using a modified definition of α' and with the exponent $\upsilon/(\upsilon + 1)$ as 2/3. The solid line is a fit using a modified definition of α' and with the exponent $\upsilon/(\upsilon + 1)$ as 4/5.

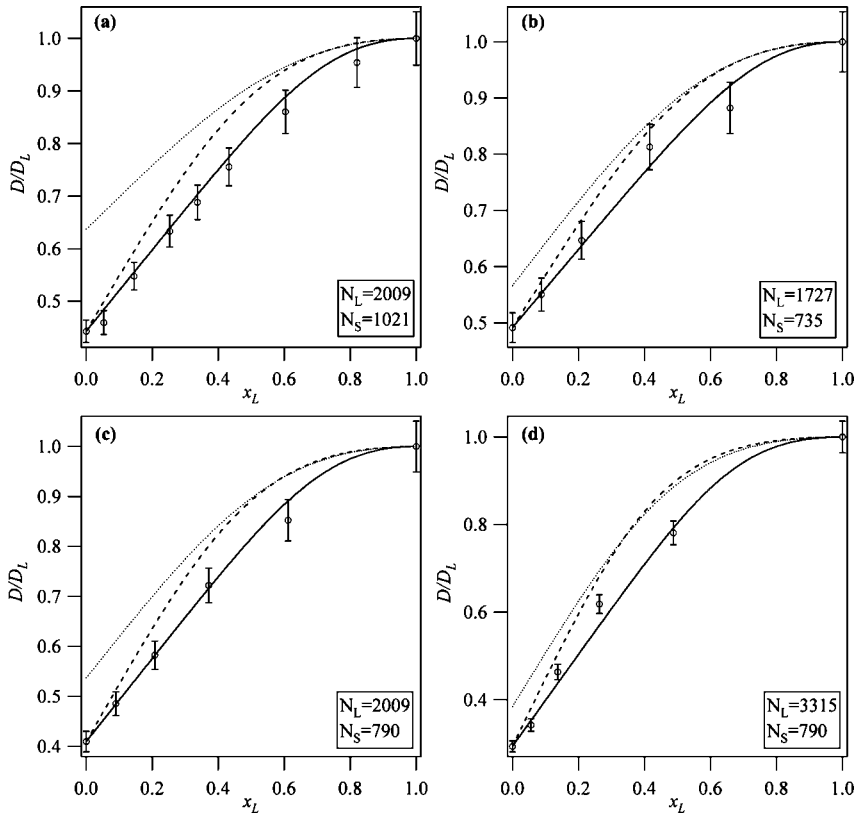

Figure 9. Lamellar period, D_{mix}, for blends where the smaller BCP is from the WSR. The dotted line is the SSR-based eq 1 with no adjustable experimental parameters. The dashed line is a fit using a modified definition of α' and with the exponent $\upsilon/(\upsilon + 1)$ as 2/3. The solid line is a fit using a modified definition of α' and with the exponent $\upsilon/(\upsilon + 1)$ as 4/5.

same BCPs were then prepared as thin (~500 nm) films on SC-ITO and annealed at 220 °C. The resulting perpendicularly oriented lamellar structures were imaged using AFM. The AFM images were PSD analyzed to prepare a spectra that could be compared to the X-ray scattering data. A typical SAXS and AFM generated spectra for 18K−18K PS-*b*-PMMA is shown in Figure 1 along with the original AFM file. There is a close correspondence of scattering peaks from both methods. The lamellar spacing for both thin film and bulk phase can be determined from the q value ($=2\pi/D$) of the principal scattering peak position, which in turn was extracted by fitting a Gaussian curve to this peak. These data are compiled and compared in Table 1 and will be shown later in Figure 3 for the four polymers that were analyzed with SAXS/USAXS. From these data we see that the thin film geometry does not significantly alter the D spacing of perpendicularly oriented BCP lamellae from the bulk phase. In comparing the SAXS and AFM generated D spacing values, we also assume that the perpendicular lamellar observed by AFM are not tilted. This is reasonable given that there is no lateral chemical patterning at the air surface that might induce tilt.[43,44] A verification of this assumption requires a 3-D characterization tool such as glancing incidence SAXS and may be the subject for future work.

13.1K–14.9K PS-*b*-PMMA is expected to have an experimentally accessible order–disorder phase transition temperature (T_{ODT}); Amundson et al. reported a T_{ODT} of 182 °C for 31K PS-*b*-PMMA.[45] Our laboratory has established an expertise in determining phase transition phenomena of BCP systems using SAXS with accurately calibrated and controlled heating apparatus.[39] This methodology was applied to determine the bulk phase T_{ODT} of 13.1K–14.9K PS-*b*-PMMA as 205 ± 3 °C.[46] In addition, thin film samples (thickness 180 nm) of 13.1K−14.9K PS-*b*-PMMA were annealed for a range of temperatures around 205 °C for an hour before being cooled quickly by immersion in LN2 to freeze in the thin film structure. The two AFM images in Figure 2 show the BCP thin film surface structure at 195 and 210 °C. Although crude in terms of temperature resolution, these images clearly indicate that a transition from the ordered to disordered phase has occurred between these temperatures. Menelle et al. reported ~50 °C shift in T_{ODT} for non-neutral surface-induced BCP phase transitions.

Through these tests, we can suggest that lamellar structures perpendicularly oriented in a BCP thin film (thicker than a monolayer) bounded by neutral boundary conditions will have the same phase separation thermodynamics as the same BCP in the bulk phase. In qualifying this statement, we associate a supercriticaly rough chemically non-neutral surface with a flat chemically neutral surface. More immediately, these findings allow us to make a direct comparison of AFM determined BCP lamellar period (from perpendicularly oriented structures) with those reported for bulk phase BCPs in previous publications or in theoretical treatments.

3.2. Lamellar Periodicity of Pure PS-*b*-PMMA Block Copolymers. Table 1 and Figure 3 show the D spacing of pure symmetric PS-*b*-PMMA determined principally from the AFM images of perpendicularly oriented lamellae. Figure 3 also includes the SAXS and USAXS determined D spacing values from the bulk phase. The data are plotted as a function of N and also χN (using χ vs temperature values determined by Russell et al.[47]). Also included in the plot are lamellar spacing information extracted from comparative texts in the literature[28,47,48] obtained from both bulk and thin film studies. These externally obtained data are purely illustrative and were not used in any quantitative analysis. Such data were typically measured at a range of different temperatures to the principal one used in this paper (220 °C). This graphical superposition is considered valid since PS-*b*-PMMA has a weakly temperature-dependent χ parameter.

On the basis of prior reports of D vs N behavior for BCPs, the experimental data in Figure 3 were fitted with a general

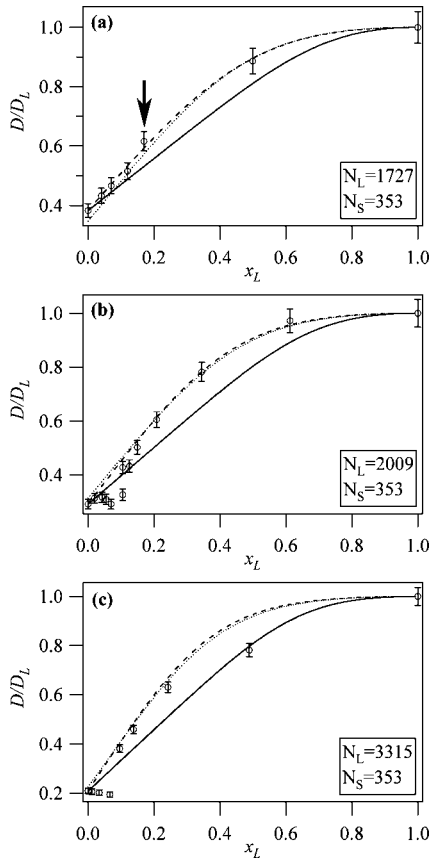

Figure 10. Lamellar period, D_{mix}, for blends where the macrophase separation occurs. The dotted line is the SSR based eq 1 with no adjustable experimental parameters. The dashed line is a fit using a modified definition of α' and with the exponent $\upsilon/(\upsilon + 1)$ as 2/3. The solid line is a fit using a modified definition of α' and with the exponent $\upsilon/(\upsilon + 1)$ as 4/5.

power law $D \sim N^u$. An exponent of 0.85 was determined for BCPs in the range of $40 < \chi N < 100$. At $\chi N > 100$, the exponent of 0.66 was extracted. On the basis of this, we have assigned the two BCPs with $\chi N > 100$ to be strongly segregating (SSR) and those with $40 < \chi N < 100$ to be of the intermediate segregation regime (ISR). Although the inclusion of two BCPs to the SSR is based on an analysis using just two data points, this conclusion was validated by the behavior of these two BCPs as blend components (described later).

It was very difficult to find a single power law behavior for the low molecular weight BCPs. We have identified a kinked D vs N behavior at these low molecular weights. There is very little experimental uncertainty in the value of D to indicate that the kink is an artifact. Indeed, as shown later in Figure 9a, it is possible to blend two BCPs: 14.9K−13.1K PS-*b*-PMMA [D = 20 nm] and 18K−18K PS-*b*-PMMA [D = 28.6 nm], from the steep slope below the kink at $N \sim 320$. The resulting lamellar structures have a mixed dimension D_{mix}, where 120 nm $< D_{mix} <$ 28.6 nm. At present, we have no satisfactory explanation for the unusual low χN trend but loosely assign BCPs where $\chi N <$ 40 to the weak segregation regime (WSR).

3.3. Blended Block Copolymers. The same AFM methodology used to analyze D vs N for pure block PS-*b*-PMMA BCPs is easily extended to the study of D_{mix} as a function of blend composition and component size allowing us to test the range of applicability of eq 1 over the WSR and ISR. However, as with pure BCPs, the thin film geometry and perpendicular orientation can lead to complications. In this case, since the perpendicular structures would contain two sizes of BCP, it is possible for entropic reasons, for one of these components to migrate up or down the perpendicular structure toward either air or substrate surface. Such surface segregation would lead to lamellae at the surfaces having a distorted dimension that would wrongly be associated with the bulk blend composition.

To explore this, we analyzed the average composition-depth profile in blended BCP thin films using dynamic SIMS. Thin film blends that included a deuterated BCP (37K–43K dPS-*b*-PMMA) component as the small BCP were prepared. Figure 4 shows the depth profiles for the pure deuterated BCP, and for blends of this with a large BCP PS-*b*-PMMA (106K−99K). In an ideal case, one expects a featureless profile consistent with bulk average compostion and no significant segregation at either air or substrate surface. The data actually show some oscillations (in both pure and blended composition profiles) that arise from some small fraction (<5%) of the thin film BCP orientation being approximately parallel. As expected, these oscillations increase in period as more of the larger BCP component is added. However, aside from the slight contribution from parallel oriented BCPs, the data show no evidence of preferential surface segregation of one BCP component. The dSIMS data in Figure 4 were fitted with a model that was developed in an earlier paper[35] for a single BCP thin film; the quality of those fits quantitatively confirms that the blended BCP has a uniform, bulk, composition distribution throughout the thin film. Although less likely to highlight slight degrees of segregation, a cross-sectional TEM image of a typical blended BCPs was obtained (Figure 5) that also indicates a continuous perpendicular structure across the thin film and allows a confident comparison of the AFM determined D spacing of blended BCP thin films to analytical predictions. These D spacing values, D_{mix}, were determined in the same manner as the pure BCP: by analyzing the 2-D averaged power spectral density (PSD) spectra of AFM images. Figure 6 shows the variation in AFM derived structure and PSD spectra of films of different composition produced by blending 18K−18K PS-*b*-PMMA and 85K−91K PS-*b*-PMMA.

In Table 2 and in Figures 7−10, D_{mix} vs blend composition data are presented for various combinations of the pure PS-*b*-PMMA BCPs used in this study. The data are arranged so that Figure 7 represents mixtures where both components are from the SSR regime; Figure 8 represents blends where the shorter BCP component belongs to the ISR regime; Figure 9 contains blends where the shorter BCP component is part of our designated WSR regime and the other component belongs to the ISR regime. Finally in Figure 10, the blends components contain the same WSR BCP component (18K−18K PS-*b*-PMMA) and an increasing longer BCP component. All the data, presented as D_{mix}/D_L, are plotted together with the SSR expression. Equation 1 plotted in each figure as a dotted line has no adjustable fitting parameter since N_L, N_S, and x_L are known *a priori*. Table 2 collates all of the raw AFM data into the various categories used for each of the four figures.

In Figure 7, it is clear that the SSR expression (dotted line) provides an excellent fit to the blend data, highlighting the success that this model has seen in previous publications.[23,24,26] This also confirms our assumption that both 106K−99K PS-*b*-PMMA and 170K−168K PS-*b*-PMMA can be included in the SSR regime. A solid line shown in the plot is an empirical fit developed and described later in the paper for blends with non-SSR components. It should be noted that this empirical fit is less satisfactory for blends of SSR BCP components.

However, from all four graphs of Figure 8, it is clear that the prediction of eq 1 shown by the dotted line fails significantly, when applied to the data from binary blends where the smallest component in the blend is not an SSR BCP. As explained in the Introduction, when either BCP component does not obey the 2/3 power law, then eq 1 will fail at $x_L = 0$. An immediate fix to this problem (at $x_L = 0$) is to introduce a new definition

Table 2. Blend Data for D_{mix} Determined from AFM Images[a]

ϕ_L	D_{mix} (nm)							
	Blends involving 2 SSR BCPs (Figure 7)							
	α=2009/3315=0.61							
0.10	100	$v/(v+1)$=0.65±0.09						
0.25	114							
0.40	116							
0.50	120							
0.60	122							
0.75	136							
0.90	139							
	Blends with small BCP component in ISR regime (Figure 8)							
	(a) α=1021/2009=0.51		(b) α=735/1727=0.43		(c) α=790/2009=0.39		(d) α=790/3315=0.24	
0.10	45.1		-		-		-	
0.20	-	$v/(v+1)$=0.85±0.04	41.1	$v/(v+1)$=0.79±0.06	47.7	$v/(v+1)$=0.82±0.04	46.9	$v/(v+1)$=0.77±0.02
0.25	53.8		-		-		-	
0.40	62.2		48.3		57.2		63.5	
0.50	67.6		-		-		-	
0.60	74.2		60.7		70.9		84.7	
0.75	84.5		-		-		-	
0.80	-		65.9		83.7		107	
0.90	93.7		-		-		-	
	Blends with small BCP component in WSR regime, large BCP in ISR(Figure 9)							
	(a) α=274/353=0.78		(b) α=353/1021=0.35		(c) α=274/1021=0.27		(d) α=353/1383=0.25	
0.10	-	$v/(v+1)$=0.68±0.16	30.6	$v/(v+1)$=0.66±0.09	-	$v/(v+1)$=0.67±0.05	-	$v/(v+1)$=0.63±.05
0.20	23.2		-		23.6		32.4	
0.25	-		32.2		-		-	
0.30	-		-		-		36.1	
0.40	24.5		33		27.7		38.8	
0.50	25.5		35.9		29.4		43.7	
0.60	25.6		36.4		30.2		-	
0.7	-		-		-		53.3	
0.75	-		38.1		-		-	
0.80	28.5		-		39.4		-	
0.90	-		40.6		-		-	
	Blends with 18k-18k PS-*b*-PMMA increasing large BCP (Figure 10)							
	(a) α=353/1727=0.20		(b) α=353/2009=0.18		(c) α=353/3315=0.11			
0.10	-	$v/(v+1)$=0. 64±0.05	30.7	$v/(v+1)$=0.67±0.02	28.2	$v/(v+1)$=0.70±0.03		
0.20	32.3		31.1		-			
0.25	-		30.3		27.7			
0.30	34.8		28.6		-			
0.40	38.5		32		26.7			
0.40	-		42		-			
0.45	-		42.5		-			
0.50	46		49.3		52.1			
0.60	-		59.4		62.9			
0.75	-		76.8		86.4			
0.80	66.2		-		-			
0.9	-		95.5		107			

[a] ϕ_L = volume fraction of large BCP component.

of α as $\alpha' \equiv (D_S/D_L)^{(v+1)/v}$ while retaining the SSR value for $v/(v+1)$ as 2/3. This has introduced two additional experimental parameters (D_L, D_S) into eq 1, rendering it semiempirical. However, as also seen by the dashed lines in Figure 8, this modification fails to adequately fit data over the entire BCP blend x_L range. It was found that allowing v as a fit parameter radically improved the fitting of the data in Figure 8. The best fit values of $v/(v+1)$ were found to vary from 0.78 to 0.85 (see Table 2, second row), indicating a slight insensitivity to the precise value of v. In Figure 8, we include visually satisfactory fits (solid line) to the data using α′ and a mean $v/(v+1)$ value of 0.82. It is not clear whether it is by chance that this $v/(v+1)$ value closely matches the power law exponent, 0.85, observed for D vs N for pure ISR BCPs.

In Figure 9 the blend pairs contain a smaller component from the WSR. Here again, eq 1 in its original form does not work (see dotted line), and it is necessary to replace α by α′. However, in these cases, the use of $v/(v+1)$ as 0.82 provides poor fits to the data (see solid lines), whereas the original SSR value of 2/3 works better (see dashed lines). For each case in Figure 9, the best-fit value of $v/(v+1)$ is given in the third row of Table 2.

In Figure 10, we have plotted the data for blends where the smaller blend component, 18K−18K PS-*b*-PMMA, is coupled to increasingly larger BCPs. It is noticeable that a discontinuity in Figure 10a (see arrow) becomes pronounced in Figure 10b,c. We consider this as evidence for macrophase separation of the two BCPs, α, within the thin film. This phenomenon is observed to occur in the bulk when α of the BCP pair was decreased below a critical value, observed and calculated to be α_c ($=N_S/N_L)_c \sim 0.2$.[21,26,49] Upon macrophase separation, the two phases usually consist of a nearly pure phase of short chain BCPs and a mixed phase consisting of short and long chain BCPs. As α decreases below α_c, the mixed phase is expected to contain a larger fraction of long chains. A novel outcome of strong macrophase separation in the thin film geometry with our perpendicular lamellar structures (e.g., Figure 9b,c) is that the air surface contains the nearly pure short chain BCP (18K−18K PS-*b*-PMMA). This is only one of the coexisting phases; the other phase must be present within the thin film.

For completeness, we have applied our empirical fitting function based on eq 1 to the portions of Figure 10 where the blend remains in a single phase. Here once again we see that the best fit is obtained when α′ is used and with $v/(v+1)$

approximately 2/3 (dashed line); the solid line represents the fit where α' is used and with $v/(v+1)$ approximately 4/5, and the dotted line is the original SSR fit provided by eq 1. The close correspondence of the dotted and dashed lines is simply because the largest two SSR BCPs and 18K−18K PS-*b*-PMMA BCP used lie along the same $N^{2/3}$ curve (see Figure 2). It thus appears that, providing a modified parameter, α', is used; this value of $v/(v+1)$ is universally applicable to all of our blends studies, except those where the smallest BCP in the blend is from the ISR regime. In that case, a value of $v/(v+1)$ as ~4/5 is more appropriate.

While BCP blends have previously been studied extensively, this paper is unique in that it reports the blending of BCPs that are not solely in the strong segregation regime. It also reports on blends used in thin films. Although Mayes et al. have looked at thin film blends using neutron reflectometry, our technique produces a greater number of data sets, collected more conveniently.

In our presented blend data, we have indicated that the existing SSR blend equation, eq 1, is indeed valid for strongly segregating PS−PMMA BCPs. However, this equation does not work when non-SSR blend components are used. Instead, we have provided two empirical improvements to eq 1. It would be interesting to see whether this model could apply to the WSRs and ISRs of other BCP blend systems. Presently, there is a lack of such published data for these regimes. For this reason, we present our findings in tabular as well graphical form to aid future investigations. Because of our bulk-comparison tests and also the observed macrophase separation in these BCP thin film blends at conditions similar to those observed in the bulk, we believe these tabular data are comparable to any future bulk blend studies.

4. Conclusions

We have used the perpendicular organization of lamellar PS-*b*-PMMA BCPs in thin films to quantitatively analyze the BCP domain period as a function of molecular weight and also as a function of blending with other PS−PMMA BCPs of different molecular weight. This is a convenient method to obtain nanostructural data that have previously been generically obtained using scattering techniques for polymers in the bulk. However, because of the thin film geometry, we qualified our results through additional tests to account for thin film factors, namely segregation effects and altered thermodynamics in the thin film.

From our AFM method, we were able to provide a comprehensive map of the D vs N behavior of pure lamellar PS-*b*-PMMA BCPs. Although there have been isolated reports in the past, our data cover a significant range of χN and show for the first time the intermediate segregation phenomena in PS-*b*-PMMA as well as indicating the region where strong segregation approximations can be applied. By using the additional data of contempory researchers, this paper also points out the existence of a sharp upturn in D vs N at low χN for presently unknown physical reasons. However, it is also well-known that PS-*b*-PMMA BCP is a remarkably subtle material and capable of manipulation in ways that have not been reported in other materials; for example, its orientation in thin films can be altered by electric, topographical, chemical, [50] and confinement effects. This flexibility also makes PS-*b*-PMMA an important technological system.

Acknowledgment. The authors thank Prof. S. Horiuchi of NAIST (Tokyo) for his kind donation of a 70K−71K PS-*b*-PMMA. E.S. thanks the Japan Society for the Promotion of Science (JSPS) and the Royal Society for their sponsorship of his research. T.H. thanks JSPS for Grant-in-Aid for Scientific Research under Grant 12305060(A) and a grant from the 21st century COE program, COE, for a United Approach to New Materials Science. E.J.K. acknowledges the support of the US National Science Foundation DMR-Polymers Program under Grant DMR07-04539. The work at UCSB also made use of MRL Central Facilities supported by the NSF MRSEC Program under Award DMR00-80034.

References and Notes

(1) Stoykovich, M. P.; Edwards, E. W.; Solak, H. H.; Nealey, P. F. *Phys. Rev. Lett.* **2006**, *97* (14), 147802.
(2) Hashimoto, T.; Yamasaki, K.; Koizumi, S.; Hasegawa, H. *Macromolecules* **1993**, *26* (11), 2895–2904.
(3) Ohta, T.; Kawasaki, K. *Macromolecules* **1986**, *19* (10), 2621–2632.
(4) Semenov, A. N. *Macromolecules* **1993**, *26* (24), 6617–6621.
(5) Hashimoto, T.; Shibayama, M.; Kawai, H. *Macromolecules* **1980**, *13* (5), 1237–1247.
(6) Hadziioannou, G.; Skoulios, A. *Macromolecules* **1982**, *15* (2), 258–262.
(7) Matsushita, Y.; Mori, K.; Saguchi, R.; Nakao, Y.; Noda, I.; Nagasawa, M. *Macromolecules* **1990**, *23* (19), 4313–4316.
(8) Papadakis, C. M.; Almdal, K.; Mortensen, K.; Posselt, D. *Europhys. Lett.* **1996**, *36* (4), 289–294.
(9) Richards, R. W.; Thomason, J. L. *Macromolecules* **1983**, *16* (6), 982–992.
(10) Xu, T.; Kim, H. C.; DeRouchey, J.; Seney, C.; Levesque, C.; Martin, P.; Stafford, C. M.; Russell, T. P. *Polymer* **2001**, *42* (21), 9091–9095.
(11) Melenkevitz, J.; Muthukumar, M. *Macromolecules* **1991**, *24* (14), 4199–4205.
(12) Rebei, A.; De Pablo, J. *Phys. Rev. E* **2001**, *6304* (4), 041802.
(13) Sones, R. A.; Terentjev, E. M.; Petschek, R. G. *Macromolecules* **1993**, *26* (13), 3344–3350.
(14) Whitmore, M. D.; Noolandi, J. *J. Chem. Phys.* **1990**, *93* (4), 2946–2955.
(15) Almdal, K.; Rosedale, J. H.; Bates, F. S.; Wignall, G. D.; Fredrickson, G. H. *Phys. Rev. Lett.* **1990**, *65* (9), 1112–1115.
(16) Mori, K.; Hasegawa, H.; Hashimoto, T. *Polymer* **2001**, *42* (7), 3009–3021.
(17) Lescanec, R. L.; Muthukumar, M. *Macromolecules* **1993**, *26* (15), 3908–3916.
(18) Matsen, M. W.; Bates, F. S. *J. Chem. Phys.* **1997**, *106* (6), 2436–2448.
(19) Hashimoto, T. *Macromolecules* **1982**, *15* (6), 1548–1553.
(20) Spontak, R. J. *Macromolecules* **1994**, *27* (22), 6363–6370.
(21) Matsen, M. W. *J. Chem. Phys.* **1995**, *103* (8), 3268–3271.
(22) Zhulina, E. B.; Birshtein, T. M. *Polymer* **1991**, *32* (7), 1299–1308.
(23) Court, F.; Hashimoto, T. *Macromolecules* **2002**, *35* (7), 2566–2575.
(24) Kane, L.; Satkowski, M. M.; Smith, S. D.; Spontak, R. J. *Macromolecules* **1996**, *29* (27), 8862–8870.
(25) Papadakis, C. M.; Mortensen, K.; Posselt, D. *Macromol. Symp.* **2000**, *149*, 99–105.
(26) Yamaguchi, D.; Hashimoto, T. *Macromolecules* **2001**, *34* (18), 6495–6505.
(27) Sivaniah, E.; Hayashi, Y.; Iino, M.; Hashimoto, T.; Fukunaga, K. *Macromolecules* **2003**, *36* (16), 5894–5896.
(28) Anastasiadis, S. H.; Russell, T. P.; Satija, S. K.; Majkrzak, C. F. *J. Chem. Phys.* **1990**, *92* (9), 5677–5691.
(29) Mayes, A. M.; Russell, T. P.; Deline, V. R.; Satija, S. K.; Majkrzak, C. F. *Macromolecules* **1994**, *27* (25), 7447–7453.
(30) Potemkin, I. I.; Busch, P.; Smilgies, D. M.; Posselt, D.; Papadakis, C. M. *Macromol. Rapid Commun.* **2007**, *28* (5), 579–584.
(31) Green, P. F.; Limary, R. *Adv. Colloid Interface Sci.* **2001**, *94* (1–3), 53–81.
(32) Lambooy, P.; Russell, T. P.; Kellogg, G. J.; Mayes, A. M.; Gallagher, P. D.; Satija, S. K. *Phys. Rev. Lett.* **1994**, *72* (18), 2899–2902.
(33) Foster, M. D.; Sikka, M.; Singh, N.; Bates, F. S.; Satija, S. K.; Majkrzak, C. F. *J. Chem. Phys.* **1992**, *96* (11), 8605–8615.
(34) Menelle, A.; Russell, T. P.; Anastasiadis, S. H.; Satija, S. K.; Majkrzak, C. F. *Phys. Rev. Lett.* **1992**, *68* (1), 67–70.
(35) Sivaniah, E.; Hayashi, Y.; Matsubara, S.; Kiyono, S.; Hashimoto, T.; Fukunaga, K.; Kramer, E. J.; Mates, T. *Macromolecules* **2005**, *38* (5), 1837–1849.
(36) Hexemer, A.; Stein, G. E.; Kramer, E. J.; Magonov, S. *Macromolecules* **2005**, *38* (16), 7083–7089.
(37) Hasegawa, H.; Hashimoto, T. *Macromolecules* **1985**, *18* (3), 589–590.
(38) Yokoyama, H.; Mates, T. E.; Kramer, E. J. *Macromolecules* **2000**, *33* (5), 1888–1898.
(39) Tanaka, H.; Hasegawa, H.; Hashimoto, T. *Macromolecules* **1991**, *24* (1), 240–251.

(40) Fujimura, M.; Hashimoto, T.; Kawai, H. *Mem. Fac. Eng., Kyoto Univ.* **1981***43* (2), 224.
(41) Hashimoto, T.; Suehiro, S.; Shibayama, M.; Saijo, K.; Kawai, H. *Polym. J.* **1981**, *13* (5), 501–516.
(42) Suehiro, S.; Saijo, K.; Ohta, Y.; Hashimoto, T.; Kawai, H. *Anal. Chim. Acta* **1986**, *189* (1), 41–56.
(43) Chen, H.; Chakrabarti, A. *J. Chem. Phys.* **1998**, *108* (16), 6897–6905.
(44) Tsori, Y.; Andelman, D. *J. Chem. Phys.* **2001**, *115* (4), 1970–1978.
(45) Amundson, K.; Helfand, E.; Patel, S. S.; Quan, X.; Smith, S. D. *Macromolecules* **1992**, *25* (7), 1935–1940.
(46) Zhao, Y.; Hashimoto, T.; Sivaniah, E. Submitted for publication, 2008.
(47) Russell, T. P.; Hjelm, R. P.; Seeger, P. A. *Macromolecules* **1990**, *23* (3), 890–893.
(48) Green, P. F.; Russell, T. P.; Jerome, R.; Granville, M. *Macromolecules* **1988**, *21* (11), 3266–3273.
(49) Hashimoto, T.; Koizumi, S.; Hasegawa, H. *Macromolecules* **1994**, *27* (6), 1562–1570.
(50) Mansky, P.; Russell, T. P.; Hawker, C. J.; Pitsikalis, M.; Mays, J. *Macromolecules* **1997**, *30* (22), 6810–6813 .

MA702465T